Optical Design and Straylight Analyses of a Spatial Heterodyne Interferometer for the Measurement of Atmospheric Temperature from Space

Martin Kaufmann[a], Konstantin Ntokas[a], Davit Sivil[b], Bernhard Michel[b], Qiuyu Chen[a], Friedhelm Olschewski[a], Oliver Wroblowski[a,d], Tobias Augspurger[a], Marco Miebach[a], Joern Ungermann[a], Tom Neubert[a], Klaus Mantel[c], and Martin Riese[a,e]

[a]Research Centre Juelich, IEK-7, Juelich, Germany
[b]Hembach Photonik, Schwabach, Germany
[c]formerly at Max-Planck-Institute for the Science of Light, Erlangen, Germany
[d]now at PTB, Berlin, Germany
[e]University of Wuppertal, Wuppertal, Germany

ABSTRACT

Spatial heterodyne spectroscopy has become increasingly attractive for remote sensing of the atmosphere from microsatellites. Its outstanding light gathering power makes this technology particularly suitable for the detection of faint signals with minimal volume requirements. This paper is about an instrument, which was designed to measure the spectral shape of an atmospheric oxygen emission. The near infrared emission is observed in limb viewing geometry from space. The optical setup and specific characteristics of the design are presented. A focus is on the straylight behaviour of the system. In-field and out-of-field contributions are discussed. Straylight kernels are applied to expected background radiation fields with regard to performance-limiting factors of the system.

Keywords: SHS, SHI, Spatial Heterodyne Spectroscopy, limb sounding, remote sensing, mesosphere, thermosphere, atmospheric temperature, satellite

1. INTRODUCTION

Spatial heterodyne spectroscopy (SHS) is a relatively new method of Fourier transform spectroscopy that offers advantages over conventional Fourier transform spectrometers in specific applications.[1–6]

The spectrometers used in SHS are called Spatial Heterodyne Interferometers (SHI). Unlike conventional Michelson interferometers, which use mirrors in their arms, SHIs use diffraction gratings. These gratings are fixed in the Littrow configuration, while one or both mirrors in a conventional Michelson interferometer are usually moving. This results in the mechanical simplicity of a static grating spectrometer combined with the high light-gathering power of interference spectrometers. In the SHS system, an additional light-gathering gain of about two orders of magnitude over conventional FTS or Fabry-Perot interference spectrometers can be achieved by field-widening using fixed prisms. These prisms are inserted between the beam splitter and the gratings. They are also necessary for converged beam configurations to maintain the imaging capabilities of the system.

The instrument described in this article is an advancement of the one described previously.[7,8] It uses an SHI to measure atmospheric O_2 A-band emissions at 762 nm in limb viewing geometry from a microsatellite. The rotational structure of that emission is used to obtain temperatures

Further author information: m.kaufmann@fz-juelich.de

CubeSats, SmallSats, and Hosted Payloads for Remote Sensing VII, edited by Sachidananda R. Babu, Thomas S. Pagano, Jeffery J. Puschell, Proc. of SPIE Vol. 12689, 1268905· © The Authors. Published under a Creative Commons Attribution CC-BY 3.0 License· doi: 10.1117/12.2677600

in the mesosphere and lower thermosphere. The relative intensities of the emission lines follow a Boltzmann distribution and the ratio of the lines can be used to derive kinetic temperature. This is made possible because the emitting molecular states are in rotational local-thermodynamic equilibrium. Satellite-borne instruments that have utilized this method for temperature derivation include, among others, OSIRIS,[9] SCIAMACHY,[10] MIGHTI,[11] and MATS.[12]

The modifications from the originally presented design include expanding the wavelength range, which now spans from 760 nm to 767 nm, encompassing the entire O_2 A-band.[13] The grating constant has been quatered, and the Littrow angle was adjusted accordingly. The Littrow wavelength is now 766.5 nm and the spatial frequency range of interferogram fringes ranges from 1 to 10 cycles/mm. The spectral resolving power (after apodization) is about 4000 using Norton-Beer strong apodization.

The optical system of the instrument consists of a front optic with a straylight baffle and an interference filter placed in front of it. Following that is a spatial heterodyne interferometer. The objective lens focuses light from the Earth limb onto the gratings of the spectrometer. After dispersion, the light is imaged onto a two-dimensional detector array by the detector optic. The entire optical system has been completely redesigned and exhibits significantly better performance than the old system.

The effective focal length of that system is 400 mm. The entrance aperture of the objective lens is circular with a diameter of 75 mm and it has a field of view of 1.3 degrees (full cone). This field of view is then imaged onto a 2-dimensional detector area of 1 cm^2.

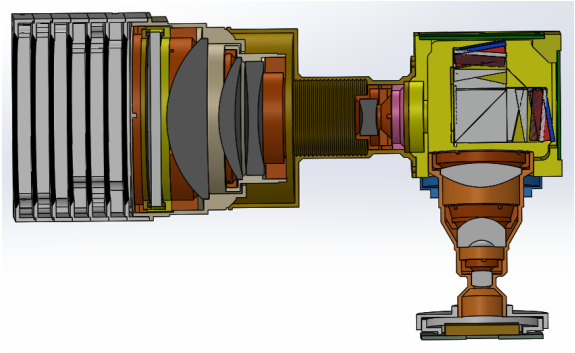

Figure 1. Light enters the instrument through the baffle and a band pass filter from the left. The front optics focuses the atmospheric scene onto the gratings of the SHI. The light is dispersed at the gratings and forms a fringe pattern. The detector optics image this fringe pattern onto a 2-dimensional detector.

2. STRAYLIGHT

In the context of employing this system for spatially-resolved measurement of spectral information, from which temperature information is subsequently derived,[14] the calibration process holds special significance.[15] This work aims to address the importance of stray light in this context, as it can introduce disturbances affecting both the spatial information and the spectral sensitivity of the measurements.

Straylight refers to any unwanted light that reaches the detector, but it is not part of the signal of interest. This can occur due to reflections, scattering, or other optical imperfections within the instrument. To address this issue, we conducted a stray light sensitivity assessment during

the design phase to mitigate its effects, wherever possible. We utilized the Advanced Systems Analysis Program Straylight (ASAP), a commercial ray tracing program that combines geometrical optical simulation with physical optics calculations. ASAP allows to identify stray light paths and characteristics effectively. To assess the current instrument, we employed forward and reverse ray tracing methods. A particular focus was on critical objects that scatter light directly towards the detector and on surfaces that receive light directly from the outside (termed 'illuminated objects'). Some components in opto-mechanics can be both critical and illuminated objects at the same time, making them potentially dangerous. In stray light analysis, it is important to identify these objects. To quantitatively evaluate the contribution of different optical and mechanical surfaces to the total straylight budget, we selectively traced only those rays that reach the detector ("importance sampling"). This was achieved by forward ray tracing the image of the detector through the system, which is called the "important edge" in ASAP terminology.

Initially, the stray light analysis was utilized to optimize the optomechanics, ensuring that it no longer exerts a significant influence on the straylight budget. The simulations indicate that, after optimization and implementing some adaptations, the peak irradiance of scattered light from the mechanics is significantly less than 1%, which is considered sufficiently low for this application.

Ghost images, resulting from internal reflections within the optical elements, superimpose on the primary image and can adversely affect the imaging quality of the instrument. Additionally, they can degrade the spatial interferogram patterns, potentially leading to inaccuracies in the spectral response of the system. For this particular instrument the main ghost is caused by a reflection at the detector surface. The light travels backward through the camera optics onto the beamsplitter and the gratings, from which it then follows the nominal path again. The peak irradiance of the main ghost is on the order of 7% of the nominal light assuming that the detector surface has 30% reflectivity, which is considered as a worst case assumption. This ghost is focused on the detector and follows the nominal light path. It can be considered as quasi-nominal light and its existence is inherent in the specific design of the SHI instrument. Other ghosts can be created at inner surfaces of the beam splitter, sharing the path of the nominal light as well. The only ghosts that lead to spatially displaced patterns are generated on the reflections on lens surfaces. However, the intenisties of these reflections are generally smaller than 0.2% of the nominal light. It can be demonstrated that none of these ghosts are major contributors that negatively impact the overall instrument performance.

The most significant source of stray light is particle contamination on the optical surfaces. At first glance, this might appear surprising, given that the instrument is assembled within ISO-class 5 cleanroom conditions, which are designed to ensure low particle contamination on the surfaces. However, when the protective cap of the optics is removed during the launch preparations, the contamination increases significantly and becomes even more pronounced the longer the instrument waits for launch. For the deployment of this instrument on a small satellite, a contamination analysis was conducted, and the anticipated particle load on the front optics was estimated. A particle contamination of 300 ppm, including contributions from the launch, is expected. This value was used in the subsequent stray light analysis. The particle size distributions were chosen according to Dittman (2002),[16] assuming cleaned surfaces.

ASAP simulations reveal that under these conditions up to 0.7% of the nominal light may end up as straylight due to scattering on particles, assuming that the light source is Lambertian and has a 2-degree angular extent. This number initially conveys limited information, as stray light sources, particularly outside the nominal field of view, are often orders of magnitude brighter than the actual signal of interest. Therefore, for further assessment of the influence of stray light, it is crucial to realistically simulate three aspects: the stray light kernels, the intensity of the signal

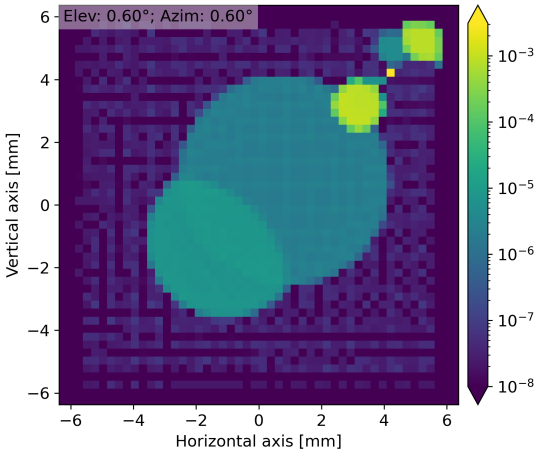

Figure 2. Example of the ghost straylight kernel captured on the detector surface at an elevation of 0.6 degrees and an azimuth of 0.6 degrees.

of interest in the nominal field of view, and the typical brightness distribution of the stray light sources in- and out of field.

For this purpose, we first calculated high-resolution stray light kernels using ASAP and then interpolated them onto a continuous grid.[17] Subsequently, we computed the expected stray light scenes for a wide range of field angles using the radiative transfer model libradtran,[18,19] which is a software package used for radiative transfer calculations in the Earth's atmospere. It allows for the calculation of spectral irradiance and actinic fluxes in the atmosphere, including effects of atmospheric constituents such as aerosols, clouds, and gases on the transmission and absorption of solar radiation. The signal of interest was simulated with an in-house non-local thermodynamic radiative transfer code.[10,13]

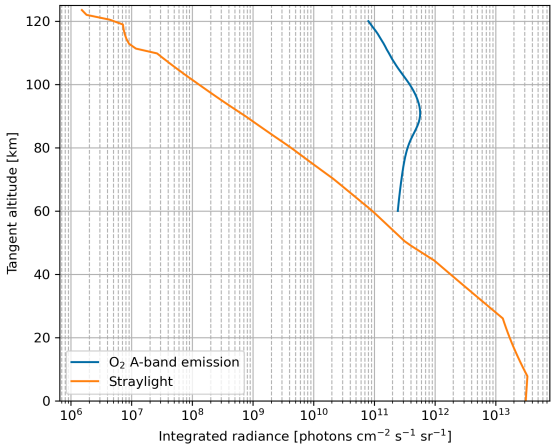

Figure 3. Integrated radiance of the O_2 A-band signal of interest along with the background radiance associated with straylight.

After convolving the straylight kernels and the stray light sources, we obtain the expected stray light for each point within the field of view, which we add to the signal of interest. As demonstrated in a more detailed analysis (Kaufmann et al., in preparation, 2023), the stray light is dominated by particle contamination on the first optical surface of the front optics and thus, it fundamentally affects both the spatial resolution capability of the instrument and the spectral modulation.

By observing the O_2 A-band, which arises from a radiative transition to the electronic and vibrational ground state of molecular oxygen, a peculiarity arises concerning the influence of stray light. That is the partial absorption of the stray light by atmospheric oxygen, resulting in a spectral signature imprinted on the straylight signal that is essentially in antiphase with the signal of interest which is an emission spectrum. How this appears in the spectral distribution of the measurement signal after Fourier transformation of the interferograms is exemplified in Figure 4.

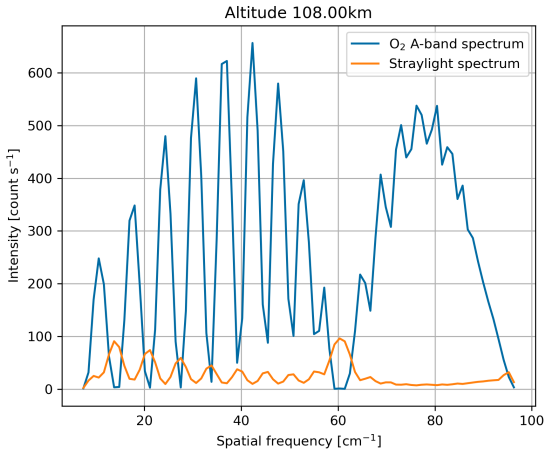

Figure 4. Signal of interest and expected straylight spectrum for a tangent altitude of 108 km

Despite this clearly visible contribution of stray light to the measurement signal, it could be demonstrated that the stray light spectrum can be effectively separated from the signal of interest over a wide range of altitudes, with minimal interference in the derivation of atmospheric temperatures. However, at both low and high altitudes, the impact of stray light surpasses that of the signal of interest, thus constraining the altitude range for the temperature data.

3. CONCLUSION

An innovative limb sounder employing a spatial heterodyne interferometer was presented for measuring spatially resolved atmospheric temperatures. Simulations were conducted to analyze the impact of stray light on the spatial and spectral sensitivity of the measurements. It has been noted that although the stray light can be efficiently mitigated from the signal at most altitudes, it does impose restrictions on the measurable altitude range, especially at higher altitudes.

It is essential to emphasize that the findings presented here are solely derived from simulations. Deviations between the actual components and the assumed conditions may result in significant variations in stray light sensitivity. As a result, laboratory measurements are currently underway, with a particular focus on studying the stray light behavior of the optomechanics and the ghosts.

To investigate the ultimate influence of particle contamination on stray light, comprehensive assessments will be conducted during the orbit phase. This will involve illuminating the instrument

from different angles using celestial objects such as the Moon. These in-orbit observations will provide crucial insights into the impact of particle contamination on stray light and will serve to validate and refine the simulation outcomes.

3.1 Acknowledgments

This project 19ENV07 MetEOC-4 has received funding from the EMPIR programme co-financed by the Participating States and from the European Union's Horizon 2020 research and innovation programme.

EMPIR EURAMET
The EMPIR initiative is co-funded by the European Union's Horizon 2020 research and innovation programme and the EMPIR Participating States

REFERENCES

[1] Connes, P., "Spectromètre interférentiel à sélection par l'amplitude de modulation," *Journal de Physique et le Radium* **19**(3), 215–222 (1958).

[2] Harlander, J., Reynolds, R. J., and Roesler, F. L., "Spatial heterodyne spectroscopy for the exploration of diffuse interstellar emission lines at far-ultraviolet wavelengths," *The Astrophysical Journal* **396**, 730 (Sept. 1992).

[3] Englert, C. R., Harlander, J. M., Brown, C. M., and Marr, K. D., "Spatial heterodyne spectroscopy at the naval research laboratory," *Appl. Opt.* **54**, F158–F163 (Nov 2015).

[4] Cardon, J., Englert, C., Harlander, J., Roesler, F., and Stevens, M., "SHIMMER on STS-112: Development and Proof-of-Concept Flight," in [*AIAA Space 2003 Conference & Exposition*], American Institute of Aeronautics and Astronautics, Long Beach, California (Sept. 2003).

[5] Watchorn, S., Roesler, F. L., Harlander, J. M., Jaehnig, K. P., Reynolds, R. J., and Sanders III, W. T., "Development of the spatial heterodyne spectrometer for VUV remote sensing of the interstellar medium," in [*UV/EUV and Visible Space Instrumentation for Astronomy and Solar Physics,*], Siegmund, O. H. W., Fineschi, S., and Gummin, M. A., eds., 284–295, Proc. SPIE 4498, San Diego, CA (Dec. 2001).

[6] Harlander, J., "Algebraic ray trace analysis of spatial heterodyne spectrometers," *Applied Optics* **62** (04 2023).

[7] Kaufmann, M., Olschewski, F., Mantel, K., Solheim, B., Shepherd, G., Deiml, M., Liu, J., Song, R., Chen, Q., Wroblowski, O., Wei, D., Zhu, Y., Wagner, F., Loosen, F., Froehlich, D., Neubert, T., Rongen, H., Knieling, P., Toumpas, P., Shan, J., Tang, G., Koppmann, R., and Riese, M., "A highly miniaturized satellite payload based on a spatial heterodyne spectrometer for atmospheric temperature measurements in the mesosphere and lower thermosphere," *Atmospheric Measurement Techniques* **11**, 3861–3870 (July 2018).

[8] Olschewski, F., Kaufmann, M., Mantel, K., Neubert, T., Rongen, H., Riese, M., and Koppmann, R., "AtmoCube A1: airglow measurements in the mesosphere and lower thermosphere by spatial heterodyne interferometry," *Journal of Applied Remote Sensing* (2019).

[9] Sheese, P. E., Llewellyn, E. J., Gattinger, R. L., Bourassa, A. E., Degenstein, D. A., Lloyd, N. D., and McDade, I. C., "Temperatures in the upper mesosphere and lower thermosphere from osiris observations of o2 a-band emission spectra," *Canadian Journal of Physics* **88**(12), 919–925 (2010).

[10] Zhu, Y. and Kaufmann, M., "Consistent Nighttime Atomic Oxygen Concentrations From O_2 A-band, O(^{1}S) Green-Line, and OH Airglow Measurements as Performed by SCIAMACHY," *Geophysical Research Letters* (2019).

[11] Stevens, M., Englert, C., Harlander, J., Marr, K., Harding, B., Triplett, C., Mlynczak, M., Yuan, T., Evans, J., Mende, S., and Immel, T., "Temperatures in the upper mesosphere and lower thermosphere from o2 atmospheric band emission observed by icon/mighti," *Space Science Reviews* **218** (11 2022).

[12] Gumbel, J., Megner, L., Christensen, O. M., Ivchenko, N., Murtagh, D. P., Chang, S., Dillner, J., Ekebrand, T., Giono, G., Hammar, A., Hedin, J., Karlsson, B., Krus, M., Li, A., McCallion, S., Olentšenko, G., Pak, S., Park, W., Rouse, J., Stegman, J., and Witt, G., "The mats satellite mission – gravity wave studies by mesospheric airglow/aerosol tomography and spectroscopy," *Atmospheric Chemistry and Physics* **20**(1), 431–455 (2020).

[13] Chen, Q., Ntokas, K., Linder, B., Krasauskas, L., Ern, M., Preusse, P., Ungermann, J., Becker, E., Kaufmann, M., and Riese, M., "Satellite observations of gravity wave momentum flux in the mesosphere and lower thermosphere (mlt): feasibility and requirements," *Atmospheric Measurement Techniques* **15**(23), 7071–7103 (2022).

[14] Ntokas, K. F. F., Ungermann, J., Kaufmann, M., Neubert, T., and Riese, M., "Observation of horizontal temperature variations by a spatial heterodyne interferometer using single-sided interferograms," *Atmospheric Measurement Techniques Discussions* **2023**, 1–24 (2023).

[15] Kaufmann, M., Olschewski, F., Mantel, K., Wroblowski, O., Chen, Q., Liu, J., Gong, Q., Wei, D., Zhu, Y., Neubert, T., Rongen, H., Koppmann, R., and Riese, M., "On the assembly and calibration of a spatial heterodyne interferometer for limb sounding of the middle atmosphere," *CEAS Space Journal* (2019).

[16] Dittman, M. G., "Contamination scatter functions for stray-light analysis," in [*Optical System Contamination: Effects, Measurements, and Control VII*], Chen, P. T. C. and Uy, O. M., eds., **4774**, 99 – 110, International Society for Optics and Photonics, SPIE (2002).

[17] Smith, W. H. F. and Wessel, P., "Gridding with continuous curvature splines in tension," *GEOPHYSICS* **55**, 293–305 (Mar. 1990).

[18] Mayer, B. and Kylling, A., "Technical note: The libradtran software package for radiative transfer calculations - description and examples of use," *Atmospheric Chemistry and Physics* **5**(7), 1855–1877 (2005).

[19] Emde, C., Buras-Schnell, R., Kylling, A., Mayer, B., Gasteiger, J., Hamann, U., Kylling, J., Richter, B., Pause, C., Dowling, T., and Bugliaro, L., "The libradtran software package for radiative transfer calculations (version 2.0.1)," *Geoscientific Model Development* **9**, 1647–1672 (05 2016).